

Dynamic Virtual Inertia and Damping Control for Zero-Inertia Grids

Oleg O. Khamisov and Stepan P. Vasilev

Abstract—In this paper virtual synchronous generation (VSG) approach is investigated in application to low- and zero-inertia grids operated by grid-forming (GFM) inverters. The key idea here is to introduce dynamic inertia and damping constants in order to keep power grid stable during different types of faults, islanding or large power balance oscillations. In order to achieve such robustness, we introduce frequency and phase angle shift functions to VSG along with dynamics virtual generator parameters. The stability of such approach is theoretically proven and theoretical results are supported by detailed case studies in RTDS (Real-Time Digital Simulator) NovaCor 1.0 with GFM inverters dynamics simulated with 1-3 microseconds timestep using two-level universal inverter model. Case studies include all aforementioned types of faults and demonstrate increased power grid robustness and survivability in comparison with traditional synchronous generation of comparable size.

Index Terms—Zero-inertia grids, Grid-forming inverters, Virtual synchronous generators, Real-Time Digital Simulator, Frequency control

NOMENCLATURE

Abbreviations

AGC	Automatic Generation Control.
IBR	Inverter-Based Resources.
PLL	Phase-Locked Loop.
RoCoF	Rate of Change of Frequency.
EMT	Electro-magnetic Transient.
GFM	Grid-Forming.
SG	Synchronous Generator.
VSG	Virtual Synchronous Generator.
PSS	Power System Stabilizer.

Variables and parameters

ω_S	Power grid frequency deviation.
θ_S	Power grid phase angle deviation.
P_G	Aggregated power grid active power generation.
P_L	Aggregated power grid active power consumption.
V_S	Aggregated power grid voltage magnitude.
G	Conductance of a line connecting inverter to power grid.
B	Susceptance of a line connecting inverter to power grid.

M_S	Aggregated power grid inertia.
D_S	Aggregated power grid dumping.
ω_{ref}	Reference frequency.
ω	Inverter VSG frequency deviation.
ω_{shift}	Inverter VSG frequency deviation shift.
ω_{set}	Inverter VSG frequency.
θ	Inverter VSG phase angle deviation.
θ_{shift}	Inverter VSG phase angle deviation shift.
θ_{set}	Inverter VSG phase angle.
P_{out}	Inverter terminal active power.
P_{ref}	Inverter reference active power.
P_{max}	Inverter maximal active power.
P_{min}	Inverter minimal active power.
γ	Filtered active power limits penalty.
τ_γ	Filter characteristic time for γ .
τ_ω	Inverter VSG characteristic time.
α	Inverter VSG inverted dumping.
α_{min}	Inverted dumping lower limit.
c_α	Inverted dumping shift coefficient.
c_θ	Inverter phase angle shift coefficient.
c_ω	Inverter frequency shift coefficient.
A	Linearized matrix of VSG dynamics.
B	Matrix with non-diagonal elements of A .
V_{out}	Inverter terminal voltage magnitude.
V_{max}	Inverter maximal voltage magnitude.
V_{min}	Inverter minimal voltage magnitude.
Q_{out}	Inverter terminal reactive power.
X	SG step-up transformer reactance.
T_q''	SG open circuit q-axis time constant
X_q'	SG q-axis transient reactance.
X_q''	SG q-axis subtransient reactance.
\mathbb{R}	Set of real numbers

Functions

$f(\theta, t)$	Inverter active power output at phase angle θ .
$f_{ref}(\theta, t)$	Inverter active power output deviation from reference power P_{ref} at phase angle θ .
$f_{max}(\theta, t)$	Inverter active power output deviation from maximal power P_{max} at phase angle θ .

I. INTRODUCTION

Integration of inverter-based resources (IBRs) into modern power grids drastically affects dynamic performances of power systems. As a result, reduced power system inertia requires faster response from frequency control algorithms. Majority of IBRs operate in grid-following control (GFL) strategy with

Oleg O. Khamisov and Stepan P. Vasilev are with Center for Energy Science & Technology, Skolkovo Institute of Science & Technology, Moscow, Russian Federation (e-mail: o.khamisov@skoltech.ru, stepan.vasilev@skoltech.ru).

Stepan P. Vasilev is with Sber AI Lab, Moscow 117312, Russia.

voltage and frequency explicitly measured in the point of interconnection with phase-locked loop (PLL) [1], [2]. This strategy is limited to grids with a significant amount of synchronous generation capable of providing adequate reference points. High penetration of GFL-based inverters is impractical and can cause instability [3], [4], [5]. As renewable energy integration increases, the focus has shifted to grid-forming (GFM) control. In this type of control IBRs create local voltage phasors and manage synchronization through frequency droop [6], allowing direct control over output frequency and active power, and similarly over voltage and reactive power [7]. Previous studies suggest that GFMs can address frequency stability issues in low inertia systems [8], [9]. Previous studies have focused on small-signal stability in systems with GFMs, often concluding the necessity of some SG presence for stability while overlooking new frequency regulation possibilities with GFMs [9]. Simultaneously, the concept of grid-forming (GFM) control ideally operates without synchronous generation. However, its practical implementation presents challenges, as illustrated in several studies [10], [11], [12]. Generally, grid-following inverters utilize a PLL for synchronization [13], whereas GFM methods are thought not to use PLL, or only for initial synchronization [12]. Nonetheless, PLL-based frequency and angle measurements can be used to enhance GFM control [14]. For parallel operation, all GFM units require synchronization, and PLL usage does not inherently conflict with GFM functionality. Power grids can operate solely with inverters using an advanced current-controlled scheme [15]. Therefore, it is not entirely accurate to claim that GFMs never use PLL [16]. Other concept of GFM control is virtual synchronous generation. Idea of virtual synchronous generation was firstly presented in [17] and is aimed to remedy the aforementioned instabilities in zero-inertia grids. The possibility of 100% GFM generation was presented in [18] with numerical simulation of corresponding EMT. Later, in [19] the authors demonstrated SG operation together with GFM. Particularly in scenarios where GFMs augment SG-driven inertial responses. Other research highlights the damping contributions of droop-controlled GFMs to frequency dynamics, typically within SG-dominated frameworks [20]. The development of control designs in this area has complications due to high standard for verifiable simulations. As it was shown in [21], standard timestep of quarter electrical cycle is usually insufficient, and detailed simulations of inverter dynamics should be done in the order of microseconds.

The main contributions of this work can be separated into 3 following items:

- 1) VSG control system that dynamically adjusts system inertia and dumping in order to maximize robustness of zero-inertia power grid.
- 2) Simulation of 100% IBR 9 bus power grid [22] with universal converter models operating at 1-3 microseconds timestep [23] implemented in RTDS NovaCor 1.0.
- 3) Detailed robustness analysis of the proposed control system, including usage of IBRs only and IBRs with SG under different system faults.

The paper is organised in the following way. Section II

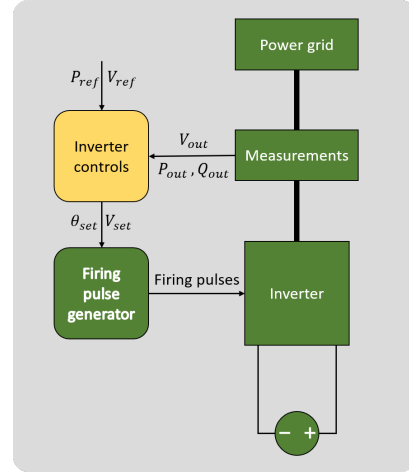


Fig. 1: Inverter setup

contains development of the VSG controller with dynamic inertia and dumping coefficients. Section III contains RTDS model of 9-bus system with possibility to switch between IBRs and SGs. Section IV is dedicated to system robustness tests. Finally section V is conclusion of the work.

II. GFM CONTROLS

This section is dedicated to the development of grid-forming inverter controls. It is assumed, that developed controller resolves measurements of voltage magnitude, actual active, reactive powers and reference values of voltage and active power (which are send by higher control loops, i.e. AGC or PSS). The controller outputs phase angle and voltage magnitude that are then used in firing pulse generator of the inverter (Fig 1). It is assumed that actual active and reactive powers (P_{out} and Q_{out}) together with voltage magnitude V_{out} are control inputs together with active power and voltage magnitude reference values (P_{ref} and V_{ref}). Then control at each point in time generates desired voltage magnitude and phase angle (V_{set} and θ_{set}) for the firing pulse generator, which, in its turn sends pulses to the inverter.

In order to improve control performance in comparison with other VSG techniques, we utilize the idea of frequency and phase angle shifts during EMT, which are impossible to introduce in SG. Their purpose is to allow the system to have large virtual inertia without violation of current limitations.

Note that active power output of inverter is defined by power flow equations

$$P_{out} = V_{out}V_S (G \cos(\theta_{out} - \theta_S) + B \sin(\theta_{out} - \theta_S)), \quad (1)$$

where G and B are conductance and susceptance respectively, V_S and θ_S are power system voltage magnitude and phase angle respectively. Since parameterise in power flows equations can vary significantly from grid to grid, for the control derivation we introduce function $f: \mathbb{R}^2 \rightarrow \mathbb{R}$ such that

$$P_{out} = f(\theta_{out}, t). \quad (2)$$

Assuming, that inverter dynamics affect insignificantly grid variables during EMT, V_S and θ_S depend on time only. Thus, its derivative in θ is given by

$$\frac{\partial f}{\partial \theta_{out}} = V_{out} V_s (B \cos(\theta_{out} - \theta_S) - G \sin(\theta_{out} - \theta_S)). \quad (3)$$

As a result, for limited difference between θ_{out} and θ_S , the derivative is positive and function f is monotonous in θ_{out} . Moreover, for transmission grids $B \gg G$ and monotonicity is kept for angle differences close to $\pi/2$. Introduction of function f will allow to derive inverter control with power grid being a black box with the monotonicity of f property.

Further control development will be separated into two subsections: control block for θ_{set} and control block for V_{set} . General control logic and its comparison with SG is given in the Fig. 2. Components for SGs are taken from [24]. Detailed description of the developed control is given in the following subsections.

A. VSG controller

The goal of VSG is to minimize frequency oscillations using second order synchronous machine dynamics, while keeping voltage within the acceptable limits. The difficulty of calculating optimal control response lays in the detailed dynamic model of power system. It is highly nonlinear and in general is non-observable and non-controllable from optimal control perspective. Thus, in this work we use a control design approach that consist of multiple simplified steps which are later verified by a detailed case study. These steps are the following:

- 1) Calculate optimal inverter power output assuming that system dynamics are aggregated to a single bus and inverter dynamics are instant;
- 2) Develop virtual inertia and dumping responses that will achieve the desired power output;
- 3) Adjust controller to account for inverter dynamics, delays in control response and measurement inaccuracies.

Let us begin with simplified problem. It is formulated as minimization of aggregated frequency deviation over classical generator model dynamics. At this step we assume, that one IBR is controlled. All other generation consists of SG and IBRs with VSG. Dynamics of all IBRs are ignored. As a result, problem statement has the following form:

$$\min \frac{1}{2} \int_0^T \omega_S^2(t) dt, \quad (4a)$$

$$M_S \dot{\omega}_S = -D_S \omega_S + P_G - P_L + P_{out}, \quad (4b)$$

$$P_{out} \in [P_{min}, P_{max}]. \quad (4c)$$

Here lower index "S" is used to emphasise that these variables are power system variables and not inverter variables. Variable ω_S is a frequency deviation from reference point, θ_S is a phase angle, P_G is generation of SGs and IBRs that are not controlled within this problem, P_{out} is power output of controlled IBR. M_S and D_S are system inertia and dumping coefficients respectively. For

$$P_G - P_L \equiv \text{const} \quad (5)$$

this problem can be solved via direct application of Pontryagin's Maximum Principle, as it was shown in [25] The solution is given by

$$P_{out}(t) = \begin{cases} P_{min}, & \omega_S(t) > 0, \\ P_{max}, & \omega_S(t) < 0, \\ P_G - P_L, & \omega_S(t) = 0. \end{cases} \quad (6)$$

While it is possible to obtain explicit solution (6), problem (4) has very strong assumption: grid topology is ignored. Moreover, it requires instant bang-bang changes in inverter power output, which are not possible to implement even with the fast inverter dynamics. Thus, we introduce VSG type of inverter control with the idea of dynamical adjustment of its parameters to achieve inverter response close to ideal one (6). Let us introduce VSG models:

$$\tau_\omega \dot{\omega} = -\omega + \alpha(P_{ref} - P_{out}), \quad (7a)$$

$$\dot{\theta} = \omega, \quad (7b)$$

$$P_{out} = f(\theta, t). \quad (7c)$$

Here P_{ref} is active power reference, obtained from outer control loop (i.e. Automatic Generation Control) and is not a part of VSG or Primary regulation control loop. For the simplicity of further derivation, VSG equation (7a) differs from actual generator swing equation (4b). This is done to analyse case, when $\alpha = 0$, which is not possible to simulate using equation (4b). Nevertheless, equation (7a) has interpretation as a generator swing equation for $\alpha \neq 0$ with virtual inertia and dumping coefficients are given by τ_ω/α and $1/\alpha$ respectively.

Now let us choose τ_ω and α in a way that allows P_{out} converge to the form (5). If system is in sliding mode we have $P_{out} = P_G - P_L$ and $\omega(t) = 0$. Thus, $\alpha = 0$ and $\tau_\omega > 0$. For the case, when control is not in sliding mode, without loss of generality it is assumed, that power grid is in power deficit and frequency is below reference value. Due to bang-bang nature of the control (6), transition to maximum power output includes discontinuity over θ in the system (7). However, θ is a solution of differential equation and is continues. In order to approximate discontinuity it is necessary to take $\dot{\theta} \rightarrow \infty$ to increase inverter power output, which yields $\omega \rightarrow \infty$ and $M \rightarrow 0$. In practice, this means transition to a zero inertia system, with step-changes in the phase angle which is highly unstable. Instead, within this work, we propose to keep system inertia significantly large and introduce limited shift to output frequency and phase angle as is shown below:

$$\tau_\omega \dot{\omega} = -\omega + \alpha(P_{ref} - P_{out}), \quad (8a)$$

$$\dot{\theta} = \omega - \omega^{shift}, \quad (8b)$$

$$P_{out} = f(\theta - \theta^{shift}, t), \quad (8c)$$

where ω^{shift} and θ^{shift} depend linearly on difference between maximal power output and actual power output. To avoid algebraic control loop and to filter measurement noise, we introduce auxiliary variable γ , which converges to linear penalty for violating active power limits as is shown below:

$$\tau_\gamma \dot{\gamma} = -\gamma + \max(0, P_{out} - P_{max}), \quad \tau_\gamma > 0, \quad (9a)$$

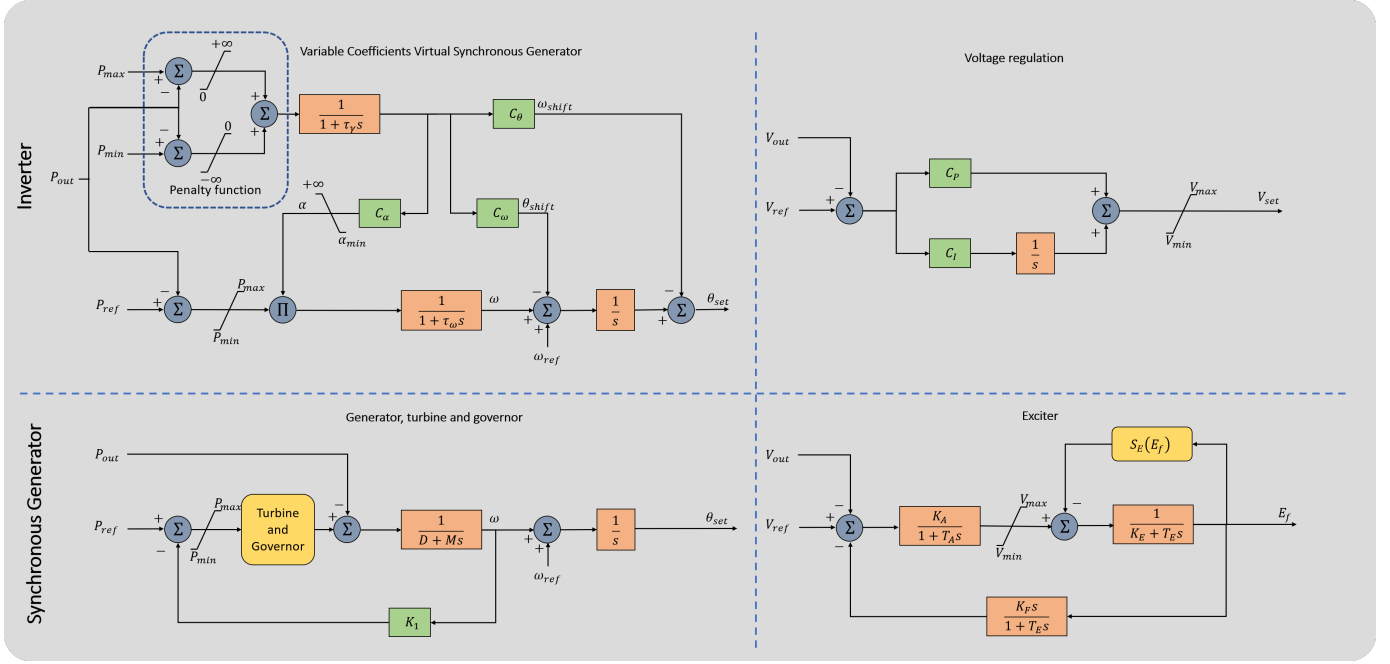


Fig. 2: Comparison of inverter and SG controls.

$$\theta_{shift} = c_\theta \gamma, \quad c_\theta > 0, \quad (9b)$$

$$\omega_{shift} = c_\omega \gamma, \quad c_\omega > 0. \quad (9c)$$

Here positive constants c_θ and c_ω are chosen to ensure stability of VSG differential equations and will be discussed later. Additionally, in the (8a) dependence on P_{ref} is present. Since it is the only inhomogeneity with respect to ω we modify it by assigning

$$\alpha = c_\alpha \gamma, \quad c_\alpha > 0. \quad (10)$$

Let us now define constants c_ω , c_θ and c_α . Recall, that function f is monotonous over θ since we assume. Thus, it is possible to introduce two monotonous functions:

$$f_{ref}(\theta, t) = f(\theta, t) - P_{ref}, \quad (11)$$

$$f_{max}(\theta, t) = f(\theta, t) - P_{max}. \quad (12)$$

This allows us to unite systems (8) and (9) into one system of differential equations (here and further it is assumed that $P_{out} \geq P_{max}$):

$$\tau_\omega \dot{\omega} = -\omega - c_\alpha \gamma f_{ref}(\theta - c_\theta \gamma, t), \quad (13a)$$

$$\dot{\theta} = \omega - c_\omega \gamma, \quad (13b)$$

$$\tau_\gamma \dot{\gamma} = -\gamma + f_{max}(\theta - c_\theta \gamma, t). \quad (13c)$$

Firstly, let us consider stationary point of this system. After excluding ω via substitution from (13a) into (13b) we get the following stationary point equations:

$$\gamma (c_\alpha f_{ref}(\theta - c_\theta \gamma, t) + c_\omega) = 0, \quad (14a)$$

$$\gamma - f_{max}(\theta - c_\theta \gamma, t) = 0. \quad (14b)$$

If $\gamma \neq 0$. Then $c_\alpha f_{ref}(\theta - c_\theta \gamma) + c_\omega = 0$ and $\gamma > 0$, since it is assumed, that $P_{out} \geq P_{max}$. Additionally, $P_{max} \geq P_{ref}$ and $f_{ref}(\theta - c_\theta \gamma, t) \geq f_{max}(\theta - c_\theta \gamma)$. As a result

$$\begin{aligned} c_\alpha f_{ref}(\theta - c_\theta \gamma, t) + c_\omega &\geq c_\alpha f_{max}(\theta - c_\theta \gamma, t) + c_\omega = \\ &= c_\alpha \gamma + c_\omega > 0. \end{aligned} \quad (15)$$

This contradiction leaves only one solution $\gamma = 0$ and $f_{max}(\theta - c_\theta \gamma, t) = 0$; thus, $P_{out} = P_{max}$ which is the desirable power output.

System (13) is nonlinear. Thus, its stability will be analyzed via linearization. The corresponding system matrix at the point $(\omega_0, \theta_0, \gamma_0, t_0)$ has form

$$A = \begin{pmatrix} -\frac{1}{\tau_\omega} & -\frac{1}{\tau_\omega} c_\theta \gamma_0 \nabla f_{ref}^0 & -\frac{c_\theta}{\tau_\omega} (f_{ref}^0 + c_\omega \nabla f_{ref}^0) \\ 1 & 0 & -c_\omega \\ 0 & \frac{1}{\tau_\gamma} \gamma_0 \nabla f_{max}^0 & -\frac{1}{\tau_\gamma} (1 + c_\theta \nabla f_{max}^0) \end{pmatrix}. \quad (16)$$

where

$$f_{ref}^0 = f(\theta_0 - c_\theta \gamma_0, t_0) \quad (17)$$

and

$$\nabla f_{ref}^0 = \left. \frac{\partial f_{ref}}{\partial \theta} \right|_{(\theta, t) = (\theta_0 - c_\theta \gamma_0, t_0)}. \quad (18)$$

Matrix A can be represented as a sum of diagonal negative semi-definite and matrix

$$B = \begin{pmatrix} 0 & -\frac{1}{\tau_\omega} c_\theta \gamma_0 \nabla f_{ref}^0 & -\frac{c_\theta}{\tau_\omega} (f_{ref}^0 + c_\omega \nabla f_{ref}^0) \\ 1 & 0 & -c_\omega \\ 0 & \frac{1}{\tau_\gamma} \gamma_0 \nabla f_{max}^0 & 0 \end{pmatrix}, \quad (19)$$

Its eigenvalues can be found via standard formula

$$\det(B - I\lambda) = \lambda \left(\lambda^2 + \frac{1}{\tau_\omega} c_\theta \gamma_0 \nabla f_{ref}^0 + \frac{1}{\tau_\gamma} \gamma_0 \nabla f_{max}^0 c_\omega \right) = 0. \quad (20)$$

Note, that γ is non-negative by definition (13c). Thus, $\gamma_0 \geq 0$. Additionally, ∇f_{ref}^0 and ∇f_{max}^0 are positive due to monotonicity and all constants $\tau_\omega, \tau_\gamma, c_\theta$ and c_ω are positive. Second summand in the brackets in (20) is non-negative, all roots λ of the equation (20) have real parts equal 0 and matrix B is negative semi-definite. Finally, matrix A also is negative semi-definite as a sum of two negative semi-definite matrices. Finally, if constants c_ω, c_θ and c_α are chosen so that

$$\det A \neq 0, \quad (21)$$

system (13) is asymptotically stable and corresponding power output converges to P_{max} .

Repeating the same approach for the lower limit P_{min} is identical to P_{max} . This statement finalizes controller derivation with a small practical adjustment. Finally, in order for the secondary frequency control regulation to operate normally, it is necessary to keep small frequency deviation even during sliding mode and VSG with dynamical inertia and dumping is represented by the following system of equations:

$$\tau_\omega \dot{\omega} = -\omega + c_\alpha \gamma (P_{ref} - P_{out}), \quad (22a)$$

$$\dot{\theta} = \omega - c_\omega \gamma, \quad (22b)$$

$$\tau_\gamma \dot{\gamma} = -\gamma + \max\{0, P_{out} - P_{max}\} + \min\{0, P_{out} - P_{min}\}, \quad (22c)$$

$$\theta^{out} = \theta - c_\theta \gamma + \omega_{ref} t. \quad (22d)$$

The exact choice of the constants $\tau_\omega, \tau_\gamma, c_\omega, c_\theta$ and c_α is empirical with respect to (21). However, during the experiments they were chosen so that virtual inertia is several times larger than inertia of comparable SG.

B. Voltage control

Idea behind voltage control is significantly simpler. It here proportional integral control is used similar to standard excitation systems:

$$V_{set}(t) = c_P (V_{ref}(t) - V_{out}(t)) + c_I \int_0^t (V_{ref}(\tau) - V_{out}(\tau)) d\tau. \quad (23a)$$

III. ZERO-INERTIA GRID SETUP

The modified IEEE 9-bus system was utilized for investigation [22]. System's generation and load parameters are presented in Table II. The table lists the capacities of inverters used as alternatives to synchronous generation. The system was tested in its traditional form with three SGs and in a modified form with an IBRs. Loads were connected to buses 5, 6, and 8. Key parameters of the 9-bus system, including line lengths, primary load capacities, and SG capacities, remained consistent. One test scenario involved adding an additional 30

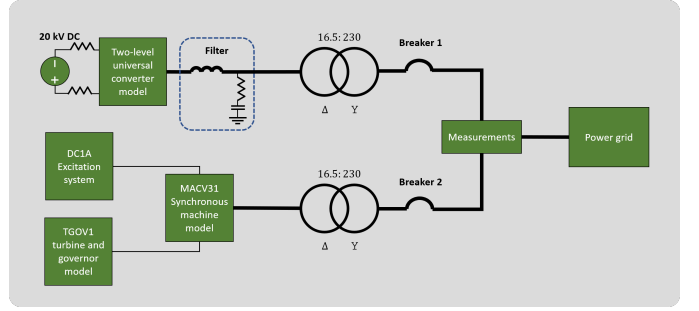


Fig. 3: Generating unit setup

TABLE I: Inertia and Dumping coefficients

	SG	Inverter
Inertia (MWs/MVAR)	23.64	25 – 100
Dumping (MW/rad)	68.95	50 – 200

MW of power to the buses with loads to observe the expected frequency drop with fully synchronous generation. In order to simulate different system setups, each generating unit is equipped with both SG and IBR (Fig. 3). Parameters of the generating units are given in Table I. Here SG damping is calculated according to the formula [24]

$$D = \frac{X'_q - X''_q}{X + X'_q} \frac{X'_q}{X''_q} T''_q V_{out}, \quad (24)$$

where X is step-up transformer reactance, T''_q is open circuit q-axis time constant, X'_q and X''_q are q-axis transient and subtransient reactances respectively.

Modeling was conducted using the Novacor 1.0 RTDS. The RSCAD model is illustrated in Fig. 4. The detailed inverter component is modeled using a substep mode with 2-5 microsecond timestep, employing a two-level substep bridge and a universal two-level converter model. The control system of the inverter immediately adopts a GFM type, integrating the Pontryagin's Maximum Principle with the VSG concept. The operation of the switches in each bridge is managed by a firing pulse generator from the RSCAD user library, which receives modulation wave inputs. The transition from the substep to the main timestep mode is carried out using substep interface transformers.

IV. SYSTEM RESILIENCE TESTS

All tests aimed to study the network operation features with partial and complete replacement of synchronous generation with an IBR. The test scenarios included:

TABLE II: Inverter-based IEEE 9-Bus System Parameters

Bus	IBR capacity (MW)	IBR capacity (MVar)	Load (MW)	Load (MVar)
1	150	200	-	-
2	250	300	-	-
3	100	200	-	-
4	-	-	-	-
5	-	-	125 + 30	50 + 0.01
6	-	-	90 + 30	30 + 0.01
7	-	-	-	-
8	-	-	100 + 30	35 + 0.01
9	-	-	-	-

- 1) Fault on line 5-7, line shutdown to eliminate the fault, and auto-reclosure of the line.
- 2) Adding additional power to the load buses.
- 3) Island mode operation of network sections when lines 5-7 and 6-9 are disconnected.

Experimental conditions:

- 1) All generation is synchronous.
- 2) One IBR, two SGs.
- 3) Two IBRs, one SG.
- 4) All IBRs.

Assumptions:

- 1) The fault type simulated is a severe three-phase to ground fault.
- 2) The functionality of protection and automation systems within the electric power system during faults is considered without detailed modeling of the underlying algorithms.
- 3) To observe the frequency sag effect, underfrequency load shedding is not simulated.
- 4) Two fault duration times on line 5-7 are simulated: 15 milliseconds (assuming correct high-speed line protection operation) and 300 milliseconds (possible in emergencies like failure of the main protection stage).
- 5) Observed system parameters: frequency, voltage, active and reactive power.

A. Load connection

Consider a scenario in which an additional 30 MW load is connected to each bus. Fig. 5 illustrates the resulting frequencies within the network. To highlight the response time of inverter-based GFM sources, a 10-second time window was selected. The frequency in a conventional 9-bus system equipped with three SGs (depicted by the blue curve) experiences a significant drop upon connection and does not recover. Conversely, as the share of IBRs in the network increases (represented by the red, green, and orange curves), the frequency recovery rate improves.

Fig. 6 and 7 present the RMS voltages, as well as the active and reactive power graphs. When compared to the initial scenario depicted in Fig. 6, which involves fully synchronous generation during additional load integration

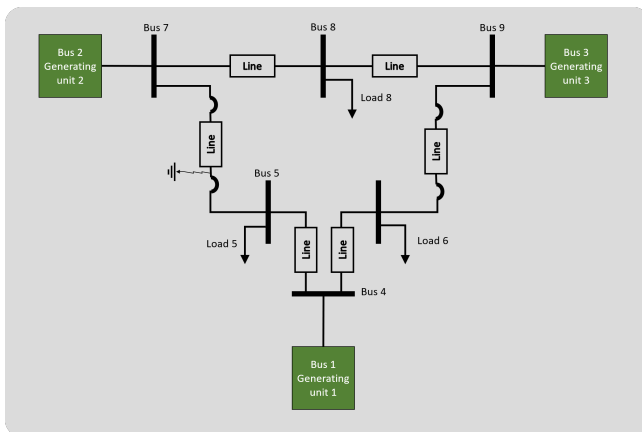


Fig. 4: 9-bus power system in RSCAD.

generation, the installation of three IBRs results in the voltages on the load buses remaining nearly constant. Additionally, the variations in the injected powers become smoother.

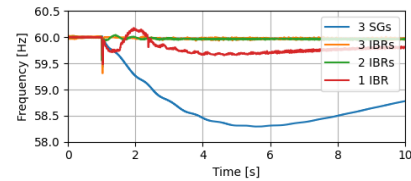


Fig. 5: Frequencies during additional load integration.

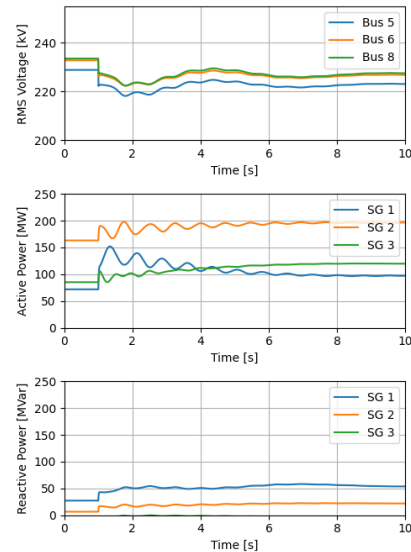


Fig. 6: Operating parameters under fully synchronous generation during additional load integration.

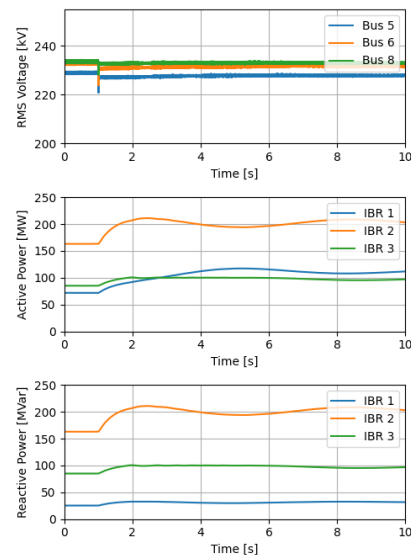


Fig. 7: Operating parameters under fully inverter-based generation during additional load integration.

B. Fault on the line 5-7

Next, we examine a scenario involving a 15-millisecond fault on line 5-7. As shown in Fig. 8, the rotational speed is better maintained with an increased share of IBR in the network, even during an emergency. While the network remains stable in all cases, the rotational speed in a fully synchronous generation scenario stabilizes in approximately 9 seconds. In contrast, with fully inverter-based generation, the rotational speed remains unaffected. Furthermore, it is noteworthy that an increased share of IBR positively influences the SGs operating in parallel with the IBRs. The transient mode duration is reduced, and the rotational speed recovers more rapidly.

Fig. 9-12 demonstrate the operating parameters as synchronous generation is sequentially replaced with IBR. There is a clear trend toward smoother transient processes and reduced recovery times for the operating parameters.

In a network configuration with one IBR and two SGs (Fig. 10), voltage recovery is faster compared to the fully synchronous generation scenario (Fig. 9). With two and three IBRs (Fig. 11 and 12), the voltage remains nearly constant.

Fig. 12 also reveals that the nature of power surges during and after the fault becomes smoother. Active power remains within 250 MW, and reactive power within 80 MVar. In contrast, the active power surge in Fig. 9 reaches up to 400 MW, with reactive power spikes up to 800 MVar. In Fig. 10 and 11, power surges are somewhat reduced. Such power

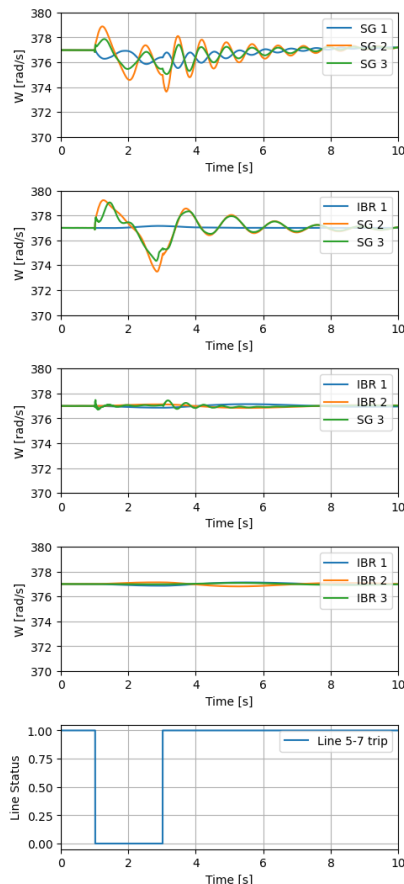


Fig. 8: Rotational speed at different generating units.

surges, as described, have the potential to damage electrical equipment.

Consider a scenario involving the abnormal operation of the protection system for line 5-7. Similar to previous cases, a fault occurs, the line shuts down, and then reclosure happens after the fault is cleared. In this instance, the fault duration is 300 milliseconds. Fig. 13 illustrates a scenario where a prolonged fault occurs in a network with fully synchronous generation. Following the fault, oscillations with an amplitude of nearly 200 kV commence. Grid fails to survive; in reality, this would result in a blackout and significant damage to the infrastructure.

In contrast, Fig. 14 presents a scenario where a prolonged

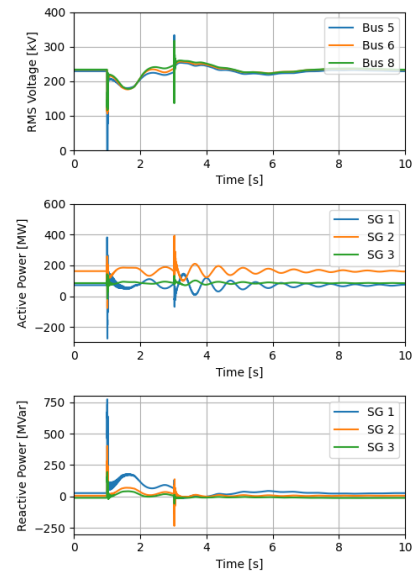


Fig. 9: Fully synchronous generation and operating parameters at fault on the line.

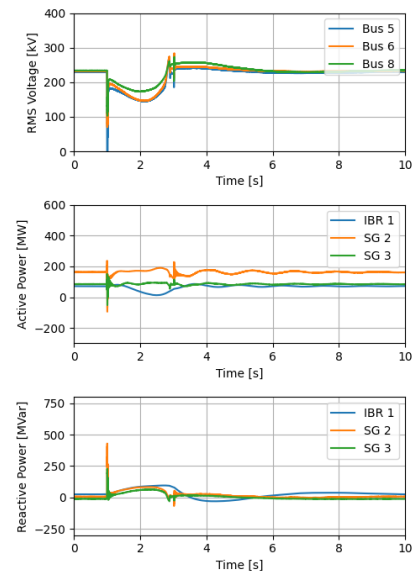


Fig. 10: One IBR, two SGs, and operating parameters at fault on the line.

fault occurs in a network with fully inverter-based generation. Despite a brief voltage surge reaching up to 400 kV and a reactive power surge up to 250 MVar once the fault is cleared, the network remains intact. This experiment demonstrates the comparative stability of an inverter-based power supply network under prolonged emergency conditions.

C. Generating unit disconnection

To further assess the reliability of the network, it is important to consider the scenario of disconnecting one of the generating units. Two cases were tested for representativeness: one with fully synchronous generation and the other with

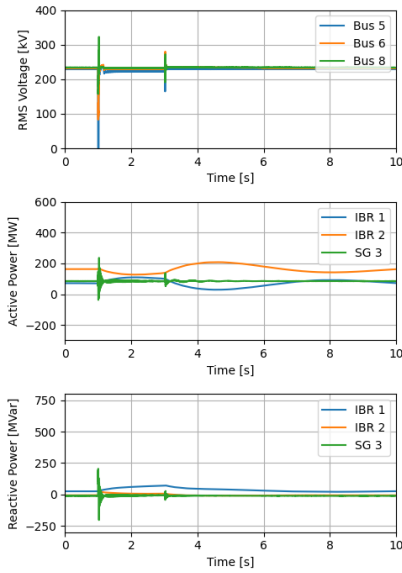


Fig. 11: Two IBRs, one SG, and operating parameters at fault on the line.

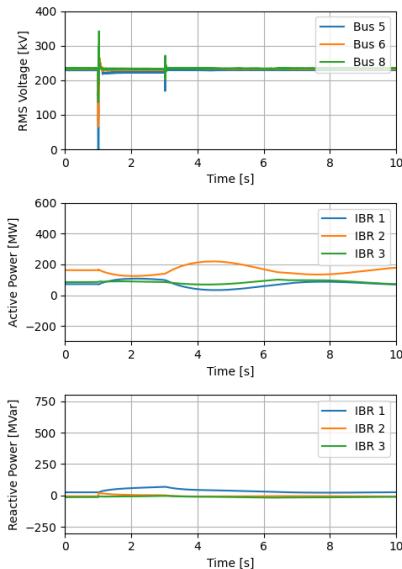


Fig. 12: Fully inverter generation and operating parameters at fault on the line.

fully inverter-based generation, with the first generating unit disconnected.

Fig. 15 shows the frequency oscillograms over a selected 20-second period for clarity. When one SG is disconnected (orange curve), the frequency drops to 57.5 Hz, which is critically low for the power system, and it does not recover, continuing to oscillate. This would lead to a system collapse in reality. Conversely, when one IBR is disconnected (blue curve), the frequency drops to 59.5 Hz but quickly recovers to its initial value.

Fig. 16 depicts the operating parameters in the case of fully synchronous generation. It shows a voltage drop to nearly 160 kV, and the power levels are unstable.

Fig. 17 illustrates the case of fully inverter-based generation, highlighting the differences in network stability.

D. Island mode

We also examine a scenario with fully inverter-based generation operating in island mode, which occurs when lines 5-7 and 6-9 are disconnected, possibly due to protection system failures or accidents. In this mode, inverters 2 and 3 supply the load on bus 8, while inverter 1 attempts to distribute power among the loads on buses 5 and 6. Fig. 18 shows that the voltage for the load on bus 8 remains stable and nearly constant. The capacities of inverters 2 and 3 are effectively distributed. However, the situation for the loads on buses 5 and 6 is different; the voltage drops to around 120 kV. Nevertheless, the network survives and continues to function in a new steady-state mode. The issue of insufficient voltage could be addressed by installing a more powerful inverter.

V. CONCLUSIONS

This paper investigates dynamics of low- and zero inertia grids with GFM inverters. Developed inverter control represents a VSG with dynamic dumping and inertia together with

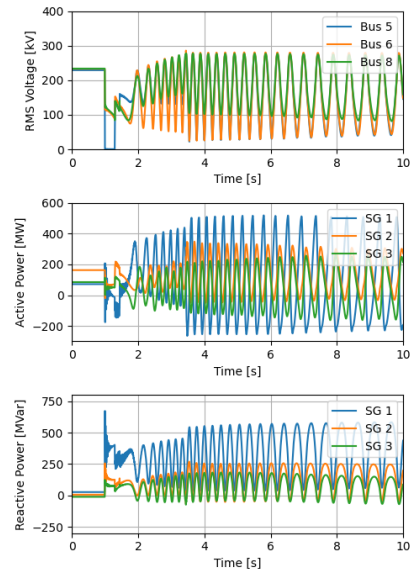


Fig. 13: Operating parameters at long fault with fully synchronous generation.

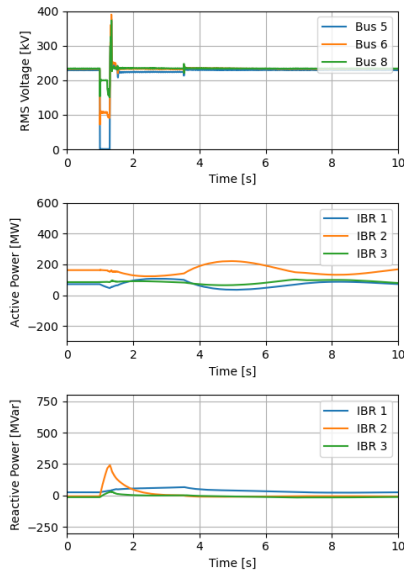


Fig. 14: Operating parameters at long fault with fully inverter generation.

additional shift functions for inverter's frequency and phase angle. The developed approach allows to keep virtual system inertia up to 4 times large and dumping up to 3 times large than the corresponding parameters of comparable SGs. Dynamic stability of the developed control approach is theoretically proven. Theoretical results are supported by extensive case study in RTDS with detailed two-level universal converter model operating at 1-3 microseconds timestep. The studies include large step-changes in loads, islanding mode and short circuits events for IEEE 9-bus case. In all experiments inverters with the developed control demonstrate superior dynamics performance and increased robustness in comparison to standard SGs.

REFERENCES

- [1] B. Kroposki, B. Johnson, Y. Zhang, V. Gevorgian, P. Denholm, B. Hodge, and B. Hannegan, "Achieving a 100% renewable grid: Operating electric power systems with extremely high levels of variable renewable energy," *IEEE Power and Energy Magazine*, vol. 15, no. 2, pp. 61–73, March 2017.
- [2] F. Milano, F. Dorfler, G. Hug, D. J. Hill, and G. Verbič, "Foundations and challenges of low-inertia systems," in *2018 Power Systems Computation Conference (PSCC)*, June 2018, pp. 1–25.
- [3] W. Wang, G. M. Huang, P. Kansal, L. E. Anderson, R. J. O'Keefe, D. Ramasubramanian, P. Mitra, and E. Farantatos, "Instability of pll synchronized converter-based generators in low short-circuit systems and the limitations of positive sequence modeling," in *2018 North American Power Symposium (NAPS)*, 2018, pp. 1–6.

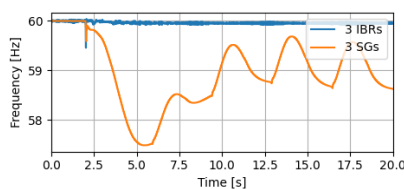


Fig. 15: Frequencies at disconnection of one generating unit in two modes.

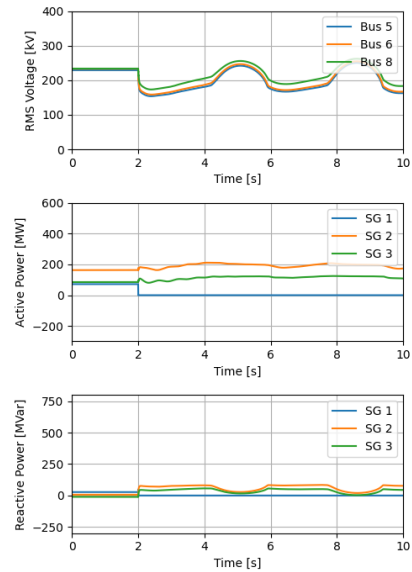


Fig. 16: Operating parameters at disconnection of one generating unit with fully synchronous generation.

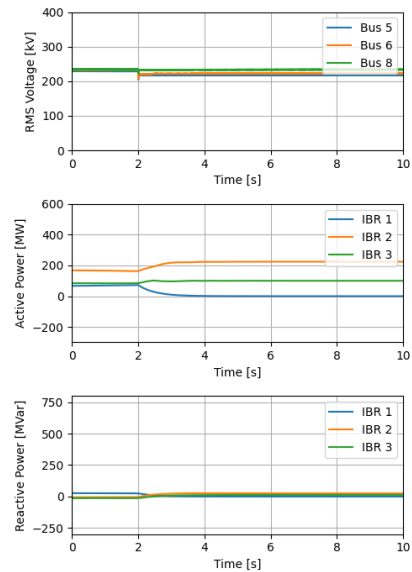


Fig. 17: Operating parameters at disconnection of one generating unit with fully inverter generation.

- [4] NERC, "Integrating inverter based resources into low short circuit strength systems," Atlanta, GA, December 2017, nERC Reliability Guideline.
- [5] Y. Lin, B. Johnson, V. Gevorgian, V. Purba, and S. Dhople, "Stability assessment of a system comprising a single machine and inverter with scalable ratings," in *2017 North American Power Symposium (NAPS)*, September 2017, pp. 1–6.
- [6] A. Sajadi, R. W. Kenyon, and B.-M. Hodge, "Synchronization in electric power networks with inherent heterogeneity up to 100% inverter-based renewable generation," *Nature Communications*, vol. 13, no. 1, p. 2490, May 2022. [Online]. Available: <https://www.nature.com/articles/s41467-022-30164-3>
- [7] NERC, "Grid forming technology: Bulk power system reliability considerations," North American Electric Reliability Corporation, Atlanta, GA, Tech. Rep., December 2021, [Online]. Available: <https://www.nerc.com/comm/RSTCReliabilityGuidelines/WhitePaperGridFormingTechnology.pdf>.

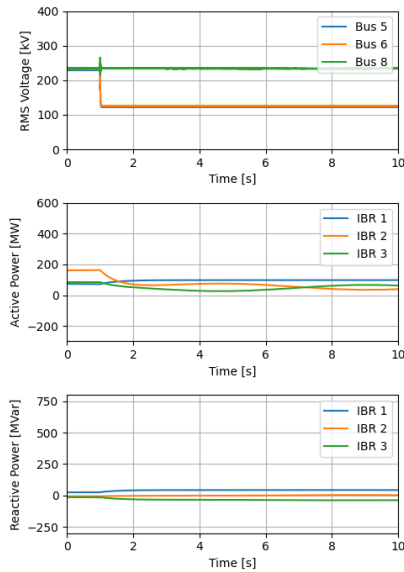


Fig. 18: Operating parameters in island mode with fully inverter generation.

- [8] Y. Lin, J. H. Eto, B. B. Johnson, J. D. Flicker, R. H. Lasseter, H. N. V. Pico, G.-S. Seo, B. J. Pierre, and A. Ellis, "Research roadmap on grid-forming inverters," National Renewable Energy Lab. (NREL), Golden, CO, Tech. Rep., 2020, tech. Rep. NREL/TP-5D00-73476.
- [9] U. Markovic, O. Stanojev, P. Aristidou, E. Vrettos, D. S. Callaway, and G. Hug, "Understanding small-signal stability of low-inertia systems," *IEEE Transactions on Power Systems*, pp. 1–1, 2021.
- [10] J. Alipoor, Y. Miura, and T. Ise, "Power system stabilization using virtual synchronous generator with alternating moment of inertia," *IEEE Journal of Emerging and Selected Topics in Power Electronics*, vol. 3, pp. 451–458, 2015.
- [11] H. Wu and X. F. Wang, "A mode-adaptive power-angle control method for transient stability enhancement of virtual synchronous generators," *IEEE Journal of Emerging and Selected Topics in Power Electronics*, vol. 8, pp. 1034–1049, 2020.
- [12] W. H. Wu, L. M. Zhou, and Y. D. Chen, "Sequence-impedance-based stability comparison between vsGs and traditional grid-connected inverters," *IEEE Transactions on Power Electronics*, vol. 1, pp. 46–52, 2019.
- [13] Q. Song, H. Zhang, K. Sun, and Y. Wei, "Improved adaptive control of inertia for virtual synchronous generators in islanding micro-grid with multiple distributed generation units," in *Proc. CSEE*, vol. 20, 2017, pp. 413–423.
- [14] L. Y. Sun, P. C. Wang, J. F. Han, and Y. Q. Wang, "Adaptive inertia control of virtual synchronous generator based on power feedback," in *Proceedings of the 2021 IEEE 4th International Electrical and Energy Conference (CIEEC)*, Wuhan, China, May 2021, pp. 28–30.
- [15] X. J. Quan, R. Y. Yu, X. Zhao, and Y. Lei, "Photovoltaic synchronous generator (pvsg): Architecture and control strategy for a grid-forming pv energy system," *IEEE Journal of Emerging and Selected Topics in Power Electronics*, vol. 8, pp. 936–948, 2020.
- [16] P. Unruh, M. Nuschke, P. Strauß, and F. Welck, "Overview on grid-forming inverter control methods," *Energies*, vol. 13, no. 10, 2020. [Online]. Available: <https://www.mdpi.com/1996-1073/13/10/2589>
- [17] H. Beck and R. Hesse, "Virtual synchronous machine," in *2007 9th International Conference on Electrical Power Quality and Utilisation*, Oct. 2007, pp. 1–6.
- [18] R. W. Kenyon, A. Sajadi, A. Hoke, and B.-M. Hodge, "Open-source pscad grid-following and grid-forming inverters and a benchmark for zero-inertia power system simulations," in *2021 IEEE Kansas Power and Energy Conference (KPEC)*, Apr. 2021, pp. 1–6.
- [19] A. Tayyebi, D. Groß, A. Anta, F. Kupzog, and F. Dörfler, "Frequency stability of synchronous machines and grid-forming power converters," *IEEE Journal of Emerging and Selected Topics in Power Electronics*, vol. 8, no. 2, pp. 1004–1018, Jun. 2020.
- [20] R. H. Lasseter, Z. Chen, and D. Pattabiraman, "Grid-forming inverters:

A critical asset for the power grid," *IEEE Journal of Emerging and Selected Topics in Power Electronics*, vol. 8, no. 2, pp. 925–935, Jun. 2020.

- [21] R. W. Kenyon, A. Sajadi, A. Hoke, and B.-M. Hodge, "Criticality of inverter controller order in power system dynamic studies – case study: Maui island," *Electric Power Systems Research*, vol. 214, p. 108789, 2023. [Online]. Available: <https://www.sciencedirect.com/science/article/pii/S0378779622008434>
- [22] P. Sauer and M. Pai, *Power System Dynamics and Stability*. Englewood Cliffs, NJ, USA: Prentice Hall, 1998.
- [23] K. Sidwall and P. Forsyth, "Advancements in real-time simulation for the validation of grid modernization technologies," *Energies*, vol. 13, no. 16, 2020.
- [24] J. Machowski, J. Bialek, and J. Bumby, *Power System Dynamics: Stability and Control*, 2nd ed. John Wiley & Sons, Inc, 2008.
- [25] O. O. Khamisov, I. Idrisov, and S. Vasilev, "Application of bang-bang control for frequency control in grids with high number of power electronics devices," in *E3S Web Conf.*, vol. 461, 2023.



Oleg O. Khamisov received M.Sc. in Applied Mathematics from Irkutsk State University, Russia in 2015 and Ph.D. in Engineering Systems from Skolkovo Institute of Science and Technology (Skoltech), Russia in 2020. Currently he is an assistant professor at Skoltech. His research is focused on development of control algorithms for low-inertia systems.



Stepan P. Vasilev received M.Sc. in Intelligent Protection, Automation and Control for Distributed Energy Systems from the Moscow Power Engineering Institute, Russia, in 2020. He is currently pursuing the Ph.D. degree with the Skolkovo Institute of Science and Technology. His research interest includes applied machine learning, power system comprehensive simulations and stability analysis.